CHAPTER III
PROTON TRACK RECONSTRUCTION: MONTE CARLO SIMULATION AND ANALYTICAL MODELS

This chapter describes the Monte Carlo simulation of the MAPS telescope. The track reconstruction is applied to the results to benchmark the telescope for proton computed tomography.

3.1 Introduction

Geant4 is a software toolkit specifically developed to simulate the interaction between particles and matter. It offers a comprehensive set of functionalities, such as tracking particles, representing geometries, modeling physics phenomena, and recording particle interactions. The toolkit covers a wide range of physics processes, including electromagnetic, hadronic, and optical processes, as well as an extensive collection of materials, elements, and long-lived particles. Geant4 is implemented in C++ and has been widely utilized in diverse fields, including particle physics, nuclear physics, accelerator design, space engineering, and medical physics.(Agostinelli et al., 2003)

The GATE software, which is an adaptation of the Geant4 toolkit, serves as a Monte Carlo simulation platform specifically designed for nuclear medicine applications (Agostinelli et al., 2003). In GATE, the simulation process has been simplified by executing it through a macro file, eliminating the need for compilation. Additional functionalities have been incorporated into the detector options, allowing for easier construction of geometries, readout operations, and trigger mechanisms. A Monte Carlo simulation was performed on the entire detector system using the GATE 9.2.0 program, which is based on Geant4 version 11.0.0. (Jan et al., 2004)

3.2 Material and method

The distance between the nozzle and the isocenter measures 42.1 cm, and the first layer of sensors is positioned at the isocenter. The telescope comprises six ALPIDE sensor planes that are spaced 25 mm apart from each other. The initial sensor

plane is located precisely at the isocenter point. This telescope design is reminiscent of the beam test facility (BTF) at Siam Research Light Institute (SLRI), which utilizes five sensor planes for characterizing ALPIDE with an electron beam (Kaewjai et al., 2019). In the case-of KCMH, an additional layer has been added to the telescope, bringing the total to six layers.

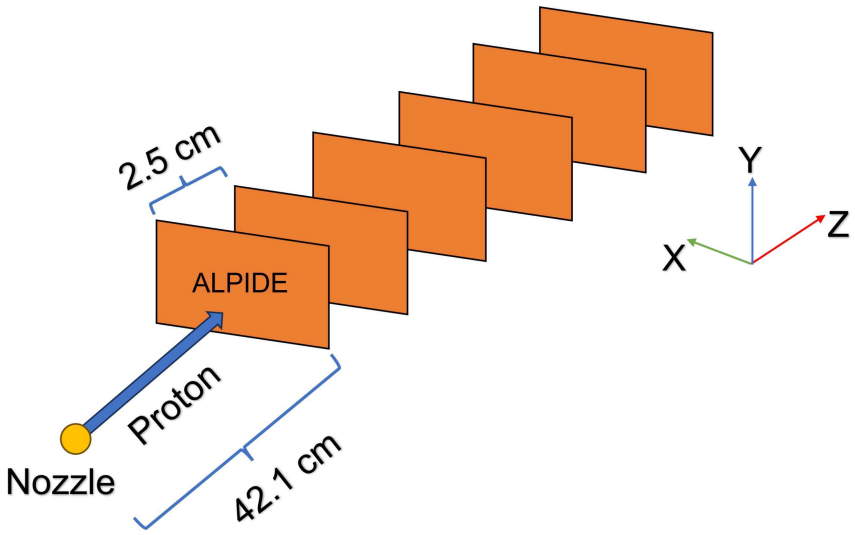

Figure 3.1 The detector geometry of MAPS telescope in GATE simulation which has 2.5 cm of air gap between each ALPIDE. The distance between nozzle and isocenter is about 42.1 cm that the first ALPIDE is located at the isocenter.

3.2.1 Layer material properties

The latest version of the ALPIDE chip is fabricated using a 180-nm CMOS imaging process and is constructed on substrates with a high-resistivity epitaxial layer, which has been thinned down to 25 μm. The chip itself has dimensions of 15 mm × 30 mm and consists of a matrix composed of 512 x 1024 pixel cells. Each pixel cell measures 26.88 μm x 29.24 μm and is read in a binary manner, indicating either a hit or no-hit (Aglieri Rinella, 2017; Yang et al., 2019), as depicted in Figure 3.2. The peripheral region of the chip, spanning 1.2 mm x 30 mm, incorporates analog biasing, control, hit-driven readout, and interfacing functionalities. The sensitive area of the chip covers 13.8 mm × 30 mm. Additionally, there exists an 11 μm metal layer positioned above the epitaxial layer, serving as the in-pixel circuitry, and facilitating the transmission of

signals and biases from the peripheral region of the chip.

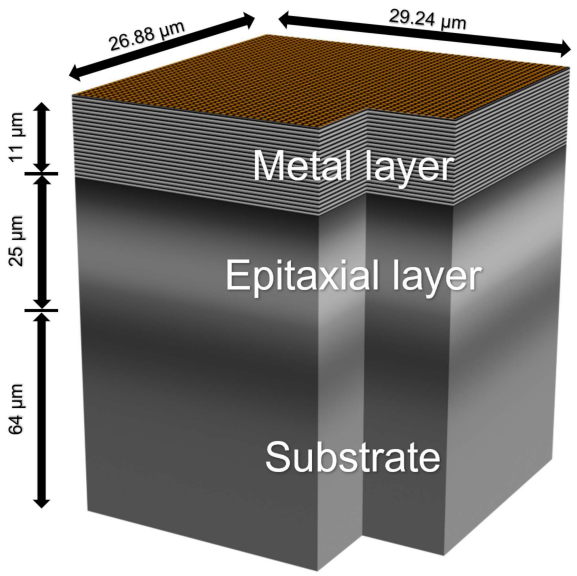

Figure 3.2 Schematic cross-section of ALPIDE.

The sensitive detector function of the epitaxial layer is achieved by incorporating the crystalSD. This crystalSD serves the purpose of monitoring interactions that take place within the volumes linked to a scanner, including crystals or collimators. It collects pertinent data regarding these interactions, such as the deposited energy, interaction location, particle source (emission vertex), type of interaction (name of the involved physical processes), and more. The attachment of a crystalSD is limited to volumes belonging to a specific system, and once attached, it remains associated with that system. The attachment process is carried out using the attachCrystalSD command. While scintillating elements (crystals) are typically the volumes to which this sensitive detector is attached, it is also possible to attach it to non-scintillating components such as collimators, shields, or septa.

3.2.2 Beam modelling

Pencil beam scanning (PBS) is an advanced technique employed in radiation therapy to precisely and accurately target tumors during treatment. Unlike traditional radiation therapy, which administers a uniform radiation dose to both the tumor and

surrounding tissue, PBS utilizes a narrow beam of radiation that is shaped and scanned layer by layer across the tumor. By adjusting the intensity and shape of the beam, medical professionals have the ability to finely control the radiation dose delivered to the tumor while minimizing exposure to healthy tissue. This approach enables the administration of higher radiation doses to the tumor, potentially enhancing treatment effectiveness while reducing side effects. PBS is typically performed using a particle accelerator like a synchrotron or cyclotron and finds frequent application in treating cancers in sensitive areas such as the brain and spine.

The Lynx PT device from IBA dosimetry is used to measure the proton beam at KCMH, as depicted in Figure 3.3. To generate this beam, the GATE PBS PencilBeam source package is employed. The primary particle type is set to protons, and their energy is measured in MeV. The distribution of particle energies within the beam can vary depending on the source and is often represented by statistical distributions such as Gaussian or uniform distributions. The pencil beam shape itself is Gaussian, and the spot sigma can be adjusted for the X-Y plane shape and angles.

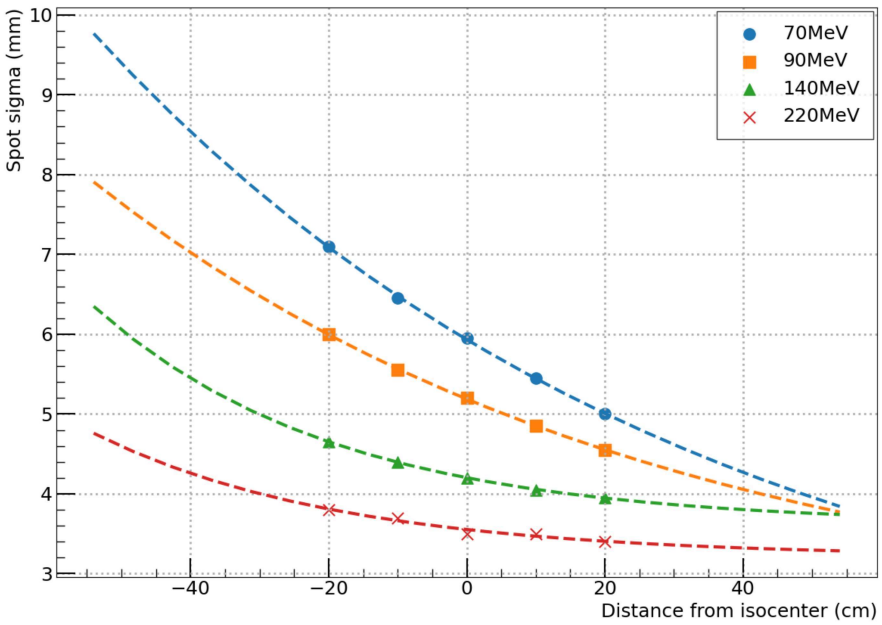

Figure 3.3 The measurement of KCMH proton beam at distance from isocenter.

3.2.3 Physics list

A physics list comprises a collection of models that describe the behavior of particles during their interactions with matter. It outlines the specific physics processes used to simulate the movement of particles through different materials, encompassing electromagnetic, hadronic, and optical processes. The physics list plays a vital role in determining various aspects of particle-matter interactions, such as energy loss, generation of secondary particles, and absorption.

Within the GATE framework, a physics list can be customized to meet the requirements of different applications. The toolkit provides a wide range of predefined physics lists tailored for various scenarios, including low-energy and high-energy physics. Users have the flexibility to select the appropriate physics list that suits their needs or even create their own custom physics list by choosing the necessary models and configuring them accordingly.

In this specific work, the simulation models employ the QGSP_BIC_EMY physics list, which includes G4EmStandardPhysics_option3 for simulating medical applications.

3.2.4 Data collection and conversion

GATE offers various output formats that can be enabled according to requirements. In this particular study, the root format is chosen. By default, the root file stores Hits Tree information, allowing event-by-event output (Brun and Rademakers, 1997). For SPECT systems, the root file contains two trees labeled as Hits and Singles. For PET systems, it includes three trees: Coincidences, Hits, and Singles. Each tree stores multiple variables relevant to the simulation.

The Hits tree encompasses numerous simulation properties that are utilized in preprocessing data for analysis in the track reconstruction algorithm. The following parameters are employed in this process.

- eventID - an identification allocated to a particular event or collision. When high-energy particles collide, a significant number of particles are produced, which are detected and recorded by a variety of detector elements such as tracking detectors, calorimeters, and muon chambers. Each recorded event provides data on the particles created by the collision, such as their momenta, energy, and other attributes.

- PDGEncoding - a unique integer value of each particle species in the Particle Data Group (PDG) particle listings. The PDG is a multinational cooperation that gathers and summarizes all known particle parameters, such as masses, lifetimes, and decay modes.

- trackID - a unique identifier of each charged particle identified in an experimental device or simulated in a computer simulation. A track is essentially a reconstruction of a trajectory in charged particle via a detector or simulation.

- parentID - an identification assigned to the parent particle that created a specific particle in a simulation or experimental measurement. This is often employed in particle collision analysis, where a high-energy particle collides with another particle, resulting in a cascade of progeny particles.

- edep - the quantity of energy deposited by a particle as it travels through a substance or a detector is referred to as energy deposition. When a particle interacts with matter, some or all of its kinetic energy is transferred to the surrounding substance. This energy deposition can have a variety of impacts on the material, such as ionization, excitation, or heating.

- posX, posY, posZ - the position of a particle in a detector or simulation along the X, Y, and Z axes. When a charged particle passes through a detector, it can generate signals in a variety of detector elements, including wire chambers, silicon detectors, and drift chambers. Physicists can reconstruct the trajectory of the particle and calculate its position and momentum by measuring the position of these signals along each axis.

- level1ID - the identifier assigned to a particle contender at the first level of trigger mechanism from a particle detector. The first level in this simulation referred to layer number of the telescope. When high-energy particles collide, a vast number of particles are produced, many of which are irrelevant to the physics study being done. Detectors often employ trigger systems to identify events of interest, which apply a series of selection criteria to detector signals to identify events of interest.

For this study, a Python script was employed to examine the conversion of raw data to root file format, allowing the collection of every event as multiple root files. Both experimental and simulation data were transformed into Pandas DataFrames to

facilitate the analysis of object-oriented data, following established conventions (McKinney, 2010). Additionally, ID properties were added to the simulation data after preprocessing to identify the particle hits for each event across all detector layers.

3.2.5 Particle track reconstruction

Particle track reconstruction is the procedure of utilizing detector data to reconstruct the paths traversed by particles through a material. It encompasses the identification and amalgamation of signals from various detector elements to reconstruct the trajectory of a particle. This is typically achieved by fitting the collected data to a mathematical model. The objective of particle track reconstruction is to precisely determine the properties of the particles, including their energy, momentum, and type, through the analysis of the detector data.

Track following algorithm

Track following is a technique widely used in particle physics to simulate the movement of particles as they traverse a detector. It entails tracing the path of the particle while it interacts with the detector material, considering deflections or changes in direction caused by scattering or other interactions. This information is crucial for reconstructing particle path and determining additional properties such as energy and charge. Sophisticated computer algorithms are typically employed for track following, taking into account various physical processes and detector characteristics. These algorithms can analyze MC simulation data to capture proton tracks from the telescope.

By utilizing 3D hit data from the telescope, it becomes feasible to reconstruct multiple particle tracks occurring simultaneously within a single data readout cycle. In a particular study, Pettersen et al. (Pettersen et al., 2020) presented algorithms for track reconstruction in a Double-Tree Cluster (DTC) detector. The approach involves a track-following and track-splitting scheme that starts from the end of the detector and progresses towards the front end, following the methodology proposed by Strandlie and Frühwirth (Strandlie and Frühwirth, 2010). The algorithm demonstrated high accuracy in detecting tracks. Further details of the algorithm are provided below.

1. Choose a hit located in the initial layer of the telescope as a seed (represented by hits in layer 0 in Subfigure (A) of Figure 3.4), potential track candidates can be

identified by searching through the remaining hits from the seed until reaching the final layer of the telescope.

2. A cone shape is employed to determine the angle between the track direction of the previous layer and the vectors connecting the previous hit and the current hit. The cone angle is evaluated using a cumulative value, S_{max}, which assesses each search angle from all potential candidates. If the cone angle is too large, the current candidates are discarded, while a smaller cone angle includes the candidate as a track (as depicted in Subfigure (B) of Figure 3.4).

3. Compute the angular deviation for each possible option in the subsequent layer and evaluate it: $S_n = \sqrt{\sum_{layer}^{n} \left(\Delta\theta_{layer}\right)^2}$ (as illustrated in Subfigure (B) of Figure 3.4), where n represents the number of layers in the telescope.

4. Gather the hits where the calculated value of S_n is less than S_{max}, designating them as part of the track (as shown in Subfigure (C) of Fig. 2.8). If multiple hits are detected, the candidate with the lowest S_n value is selected as the new segment of the track (depicted in Subfigure (D) of Figure 3.4).

5. Repeat the aforementioned procedure and continue tracking all candidates using a recursive algorithm (as depicted in Subfigure (E) of Figure 3.4) until the final layer is reached during the search process.

6. Remove the hit members of the fully reconstructed track from the hit data and repeat the process of selecting a seed from layer 0 once more (as shown in Subfigure (G) of Figure 3.4). Run the track reconstruction algorithm again to obtain new tracks until there are no more seeds remaining on the first layer (depicted in Subfigure (H) of Figure 3.4).

Searching cone

As outlined in previous subsection, the region for searching and collecting track candidates is specified as the intersection between a cone shape and the plane of the detector. This process is visually represented in Figure 3.5, where the estimated position can be precisely determined.

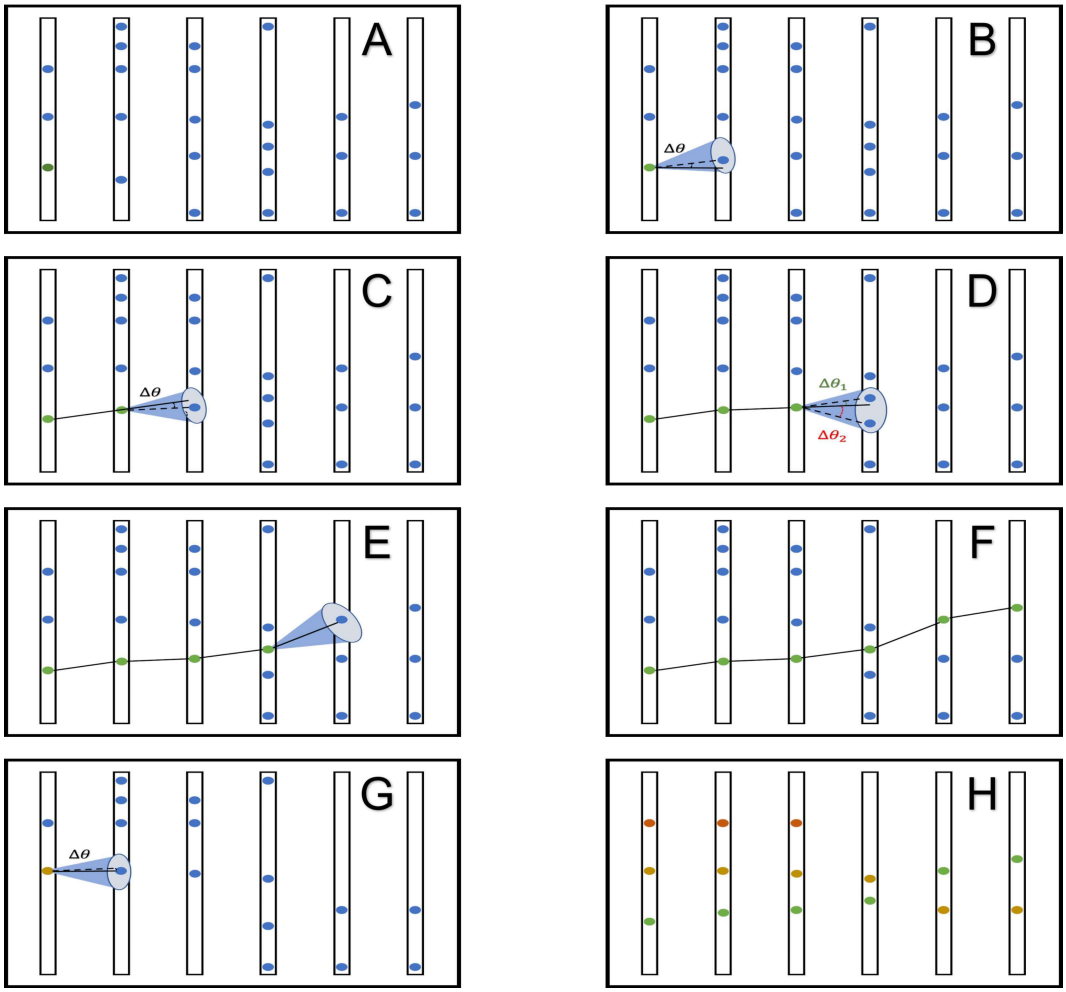

Figure 3.4 The diagram illustrates the sequence of steps in the tracking algorithm. Hits in different layers of the detector are depicted as blue dots. The process begins by selecting the first hit of a track (highlighted in green) from the first layer (A). Next, candidates for the track are searched using a cone defined by S_{max} (B). If the calculated S_n for a new candidate is lower than S_{max}, the hit is added to the track (C). If multiple hits are identified, the candidate with the lowest S_n value is selected (D). These steps are repeated for the subsequent layers (E) until the last layer of the detector is reached (F). Afterward, hits belonging to this track are removed from the pool of hits, and the reconstruction of the next track begins (G). The algorithm continues until all identified tracks are successfully reconstructed (H).

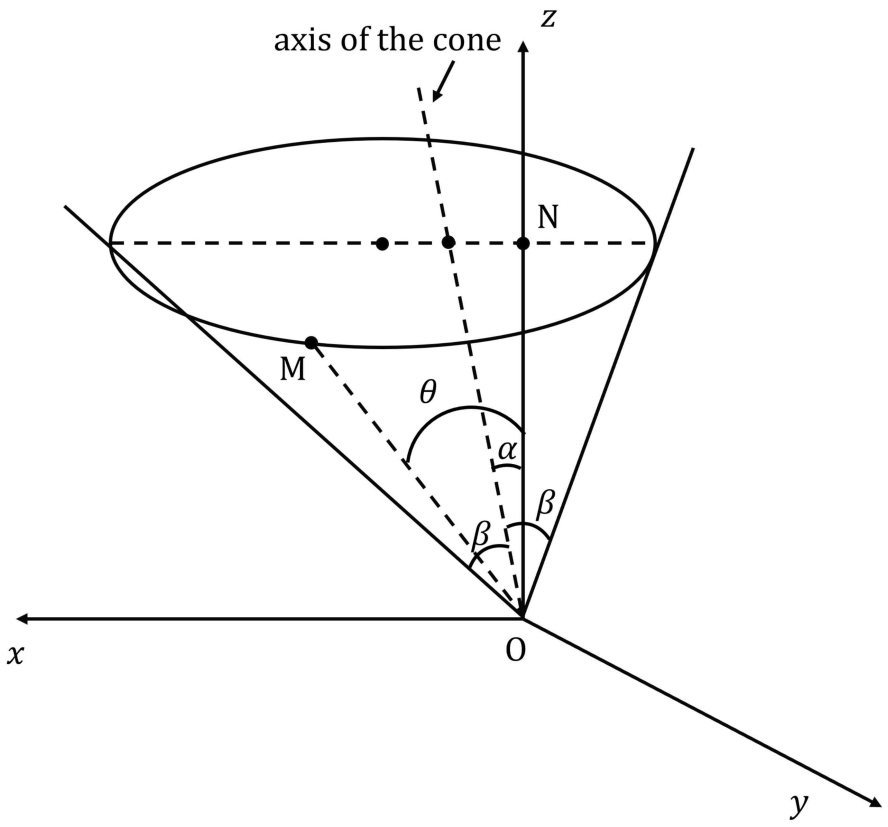

Figure 3.5 The cone intersects C(0,0;α,δ,θ) with a horizontal plane where z > 0, the resulting shape is an ellipse. The major axis of the ellipse aligns with the x-axis, while the minor axis aligns with the y-axis. (Maxim et al., 2009).

$$\begin{cases} x = z\dfrac{\sin\alpha\cos\alpha}{\cos^2\alpha - \sin^2\beta} + \dfrac{\sin\beta\cos\beta}{\cos^2\alpha - \sin^2\beta}\cos\varphi \\ y = z\dfrac{\sin\beta}{\sqrt{\cos^2\alpha - \sin^2\beta}}\sin\varphi \\ z = z \end{cases} \tag{3.1}$$

where:

- $z \geq 0$ indicates to detector layer

- β corresponds to the the expected proton scattering. The Box-Muller transform

(Box and Muller, 1958) is used to calculate this value, that generated by a standard normal distribution with $\sigma = \theta_0$ from Higland equation (Eq. 3.4) as the equation require the information of material layer described in chapter 3.2.1.

- $\varphi \in [0, 2\pi)$ is represented as the intersection between the cone C(0,0;α, 0,β) and the flat plane including M point.

- α is defined as the angle between previous direction and Oz vector: $\alpha = \cos^{-1}\left(\frac{dz}{x^2 + y^2 + dz^2}\right)$ where dz represented to the gap between layers, in this case, 25 mm.

For the remaining sensor layers, the cone will be denoted as C(0,0;α,σ,β), with σ representing the angle between the major axis of the ellipse and the Ox axis, as depicted in Figure 3.6.

Consequently, x and y of new coordinate system of equation3.1 with cone rotation should be replaced by x' and y' respectively as below.

$$\begin{cases} x' = x\cos\sigma + y\sin\sigma \\ y' = -x\sin\sigma + y\cos\sigma \\ z = z \end{cases} \tag{3.2}$$

A new cone C(0,0;α,σ,β) is computed for every layer to determine the x and y coordinates of the particle at each interaction until the final layer is reached.

Scattering angle

The track reconstruction algorithm, illustrated in Figure 3.4, involves regenerating the search cone each time a new candidate is found. In the algorithm, the S_{max} value remains constant to determine which hits are considered as candidates. The square root of the sum of squared angles between the current hit and the previous hit is calculated as

$$S_n = \sqrt{\Sigma_{layer}^{n} \left(\Delta\theta_{layer}\right)^2}, \tag{3.3}$$

where n is the total number of detector layers, and $\Delta\theta_{layer}$ represents the angle between the track direction on the current layer and previous direction of this track.

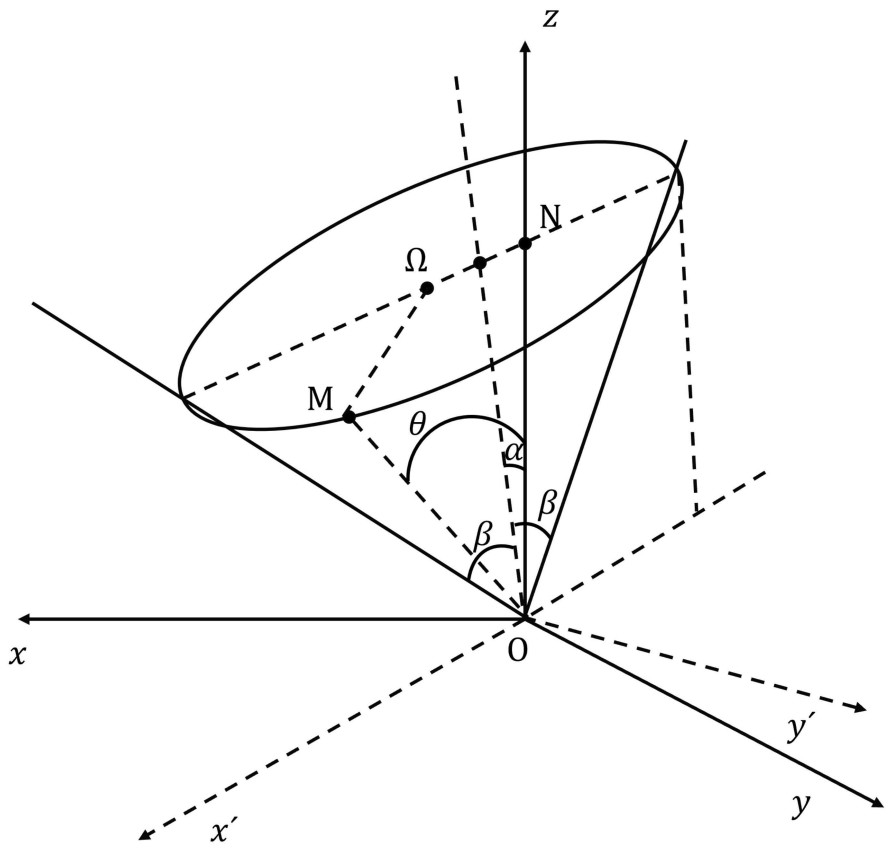

Figure 3.6 The angular parameters, α and σ, define the arbitrary direction of the cone axis, while β represents the cone opening. The intersection between the cone and a horizontal plane with z > 0 forms an ellipse $E(z; \alpha, \sigma, \beta)$. The major axis of the ellipse is inclined at an angle to the 0x axis (Maxim et al., 2009).

According to Equation 3.3, a hit that provides S_n value smaller than S_{max} is account to a track candidates. The $\Delta\theta$ in the track algorithm can be estimated Gaussian approximation by calculating the sigma value of Highland's equation (Highland, 1975) as

$$\sigma_{\theta_0} = \frac{14.1\text{MeV}}{pv}\sqrt{\frac{x}{X_0}}\left(1 + \frac{1}{9}\log_{10}\frac{x}{X_0}\right), \tag{3.4}$$

where p is particle momentum, v is particle velocity, X represents material thickness, and X_0 represents radiation length.

Radiation Length

Radiation Length is the distance over which the energy of a high-energy particle is reduced to 1/e (about 37%) of its initial value due to bremsstrahlung. Bremsstrahlung is the electromagnetic radiation emitted by a charged particle when it is accelerated by another charged particle or a nucleus. The radiation length is a material parameter that is affected by the substance that the particle is travelling through. It is denoted as X_0 which is typically calculated using the following equation:

$$X_0 = \frac{716.4A}{Z(Z+1)\ln\left(\frac{287}{\sqrt{Z}}\right)} \, g/cm^2 \tag{3.5}$$

where A represents the atomic mass of the material and Z represents the atomic number. In high-energy physics research, X_0 is a significant parameter as it determines the amount of energy deposited by a high-energy particle as it traverses a material. Typically, X_0 values for most materials range from millimeters to centimeters. In composite materials, the radiation length can be computed using the following method:

$$\frac{W_0}{x_0} = \sum \frac{W_i}{x_i}, \tag{3.6}$$

where W_0 is total mass of the sample in $g \cdot cm^2$, X_0 is combined radiation length of the sample in $g \cdot cm^2$, and W_i represents radiation length of the individual component in $g \cdot cm^2$.

The ALPIDE sensor is composed of multiple material layers, including aluminum (Al) for the metal layer, silicon (Si) for the epitaxial and substrate layers. Table 3.1 provides the radiation length property for each of these material layers in the ALPIDE sensor (source:http://pdg.lbl.gov/2009/AtomicNuclearProperties/). The radiation length of composite layers can be determined using Equation 3.6. Additionally, the radiation length of the ALPIDE sensor with a thickness of 50 μm can be obtained from the work by (Abelev and ALICE Collaboration, 2014).

Linked list structure

The track reconstruction approach is developed using linked lists for recursion programming and resource conservation in object oriented programming. Each hit data in a sensor layer is linked together as a linked list. The representation of hits data is

Table 3.1 The radiation length of material layers of ALPIDE sensor.

Layer	Material	Thickness (μm)	X_0 (cm)
Metal	Al	11	8.897
Epitaxial	Si	25	9.370
Substrate	Si	64	9.370
ALPIDE	Al + Si	100	9.307
*ALPIDE (50 μm)		50	9.369

referred to as a node. Each node holds the information provided in section 3.2.4 , and additive data is computed for insertion into the hit node. As shown in Figure 3.7, the in-layer linked lists of 6 layers are layered in the detector linked list, which binds the first hit in the current layer to the first of the next layer. The additional information is provided below.

- ID - the unique integer value that is assigned to every hits. In the reconstruction algorithm, the searching process observes every hits at a time. So, the ID is defined to help the search identifying individual hit.
- S_n - the value that is calculated by $S_n = \sqrt{\sum_{layer}^{n} \left(\Delta\theta_{layer}\right)^2}$ to compare with S_{max} value to cut off candidates.
- dvector - the different angle between search cone and the vector of current hit and next hit.

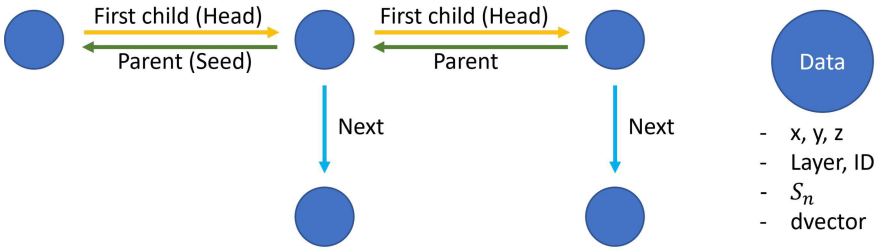

Figure 3.7 The linked list structure of the track reconstruction which used for recursive algorithm and low resources consumption.

The physical location of data pieces in memory is not used to arrange them in a linear collection. Instead, each piece refers to the one preceding it. This data structure is known as a linked list, and it is made up of nodes that form a series. Each node in the sequence carries data as well as a reference (or link) to the next node in the sequence. This structure, in its most basic version, allows for the efficient addition or removal of items from any place in the sequence. More complex forms may incorporate more links, allowing for even faster insertion and removal at arbitrary points.

Track efficiency

In order to assess the effectiveness of reconstructing a charged particle in a Monte Carlo (MC) simulation, the hits generated in the silicon tracker are utilized for track reconstruction. This reconstructed track is then compared with the original track to determine the success of the reconstruction. The overall efficiency is divided into acceptance and reconstruction efficiency for the purpose of this study. Acceptance refers to the probability that a charged particle will produce a sufficient number of hits in the tracker, allowing it to be successfully reconstructed by the track-finding algorithm. On the other hand, reconstruction efficiency measures the probability that these hits will be utilized to accurately reconstruct a track with parameters similar to those of the original particle. Acceptance takes into consideration factors such as detector geometry, material properties, and the performance of the silicon sensors. Efficiency is influenced by the specific track-finding algorithm employed and the hit occupancy, which is affected by the presence of low-momentum particles that are challenging to precisely simulate (CMS, 2010). The track efficiency is calculated as

$$\text{eff} = \mathcal{A} \cdot \epsilon = \frac{N_{\text{reco,iso}}}{N_{\text{gen}}} \cdot \frac{N_{\text{reco,embed}}}{N_{\text{reco,iso}}}, \tag{3.7}$$

where N_{gen} represents the total number of tracks simulated, $N_{\text{reco,iso}}$ represents the count of simulated tracks that are correctly reconstructed, and $N_{\text{reco,embed}}$ represents the count of tracks correctly reconstructed both in the data and the simulation. The primary criterion for determining the successful reconstruction of a track in this study is based on a threshold of 100% hit association between the reconstructed track and the simulated charged particle for the telescope used.

3.3 Results and discussion

3.3.1 Beam profile

As stated in section 3.2.2, the primary source utilized in this simulation consists of Gaussian beams with energy levels of 70 MeV and 200 MeV. As the proton beam travels through the air, it spreads, resulting in an increased sigma spot and modified beam shape. The telescope detector is employed in this simulation to observe the beam profile. The analysis reveals that the size of the beam spot grows at intervals of 2.5 cm between each sensor. The findings presented in this section illustrate the beam profile of both the 70 MeV and 200 MeV pencil proton beams as detected by the telescope detector.

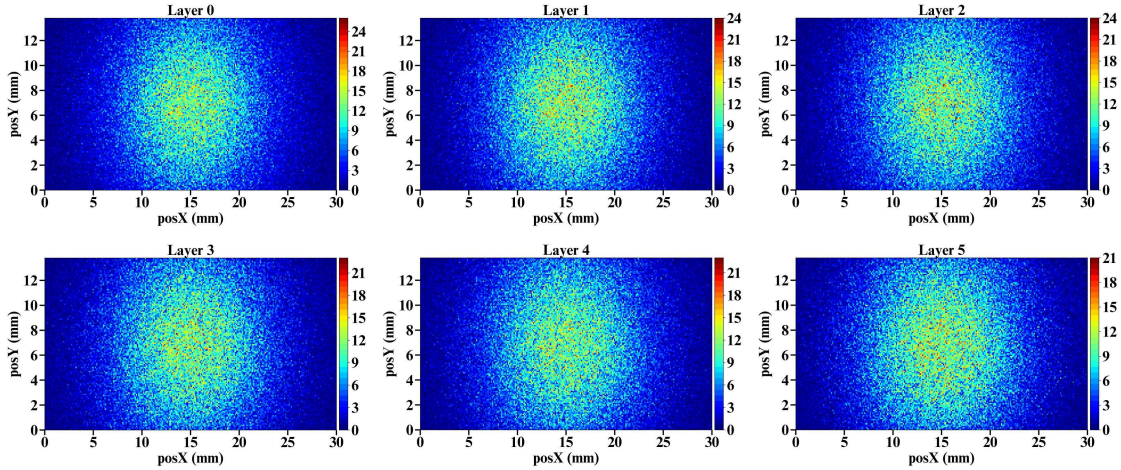

Figure 3.8 The beam profile of 70 MeV pencil proton beam in 200000 events. The color bar of the histogram shows the entries of proton hit on specific point of ALPIDE sensor.

According to figure 3.8 and table 3.2, the spot beam profile of 70 MeV shows that the center of the beam is in the center of every detector layer. The sigma in X direction is comparable to KCMH beam measurement that has described in section 3.3, but the Y axis indicates the inconsistency of sigma because of oversized beam on that axis. So, by using the beam characteristics for modeling beam profile in Gaussian model, the ideal beam profile can be represented as in figure 3.9.

Based on the information provided in Figure 3.10 and Table 3.3, the Gaussian beam profile of 200 MeV beam can be calculated similar to 70 MeV source. But, the

Table 3.2 The simulated beam characteristics of 70 MeV pencil proton beam.

Plane no.	Mean X (mm)	Mean Y (mm)	sigma X (mm)	sigma Y (mm)
0	0.029228	-0.007334	5.498986	3.604242
1	0.030752	-0.009686	5.562324	3.613843
2	0.031516	-0.010166	5.625496	3.620563
3	0.028350	-0.010087	5.692872	3.626612
4	0.027526	-0.009466	5.760172	3.631103
5	0.031726	-0.007003	5.829004	3.636043

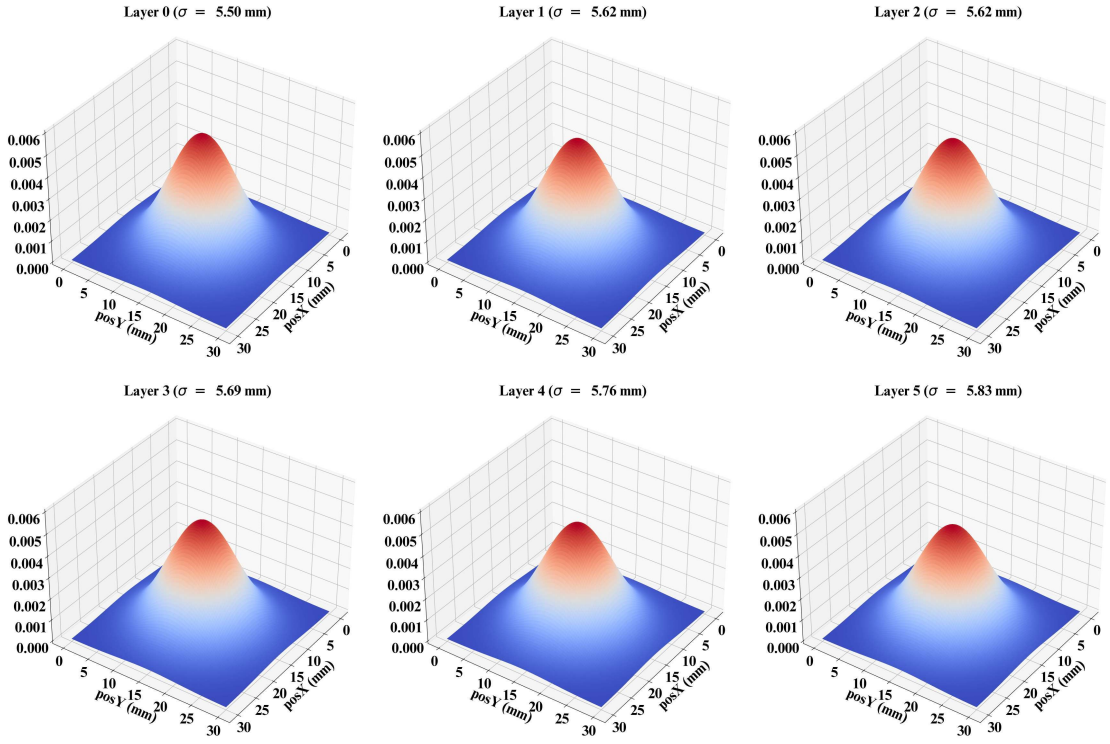

Figure 3.9 The 70 MeV pencil proton beam modeled by Gaussian distribution. The fitting parameters are calculated as shown in Table 3.2.

beam fit of Y axis still mismatch with KCMH data because of losing some hit data in that axis . The ideal beam profile can be represented as shown in Figure 3.11.

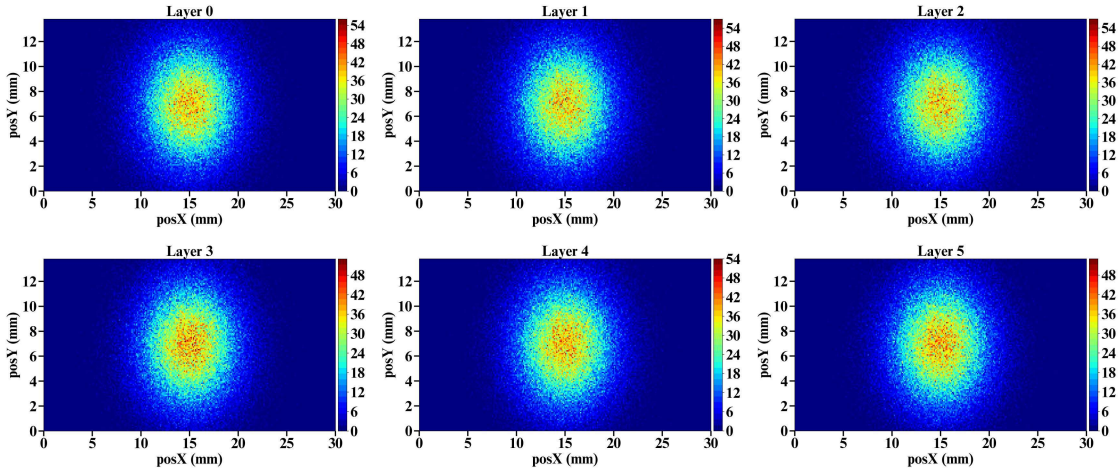

Figure 3.10 The beam profile of 200 MeV pencil proton beam in 200000 events. The color bar of the histogram shows the entries of proton hit on specific point of ALPIDE sensor.

Table 3.3 The simulated beam characteristics of 200 MeV pencil proton beam.

Plane no.	Mean X (mm)	Mean Y (mm)	sigma X (mm)	sigma Y (mm)
0	-0.006722	-0.001962	3.246739	2.919203
1	-0.006517	-0.002003	3.249379	2.920486
2	-0.006570	-0.002322	3.251722	2.921759
3	-0.006691	-0.002437	3.254626	2.922672
4	-0.006516	-0.002126	3.257421	2.923582
5	-0.006387	-0.002503	3.260514	2.924530

3.3.2 Energy deposition

When a high-energy particle travels through a detector, it can cause a chain reaction of secondary particles to deposit energy in the detection material. Physicists can reconstruct the energy and momentum of the original particle by measuring the total energy deposited in the detector. The proton energy source can deposit energy into the material it passes through, as well as secondary particles formed by the interaction of the primary source with matter. The simulation helps to determine the deposited energy in each epitaxial layer of each ALPIDE plane.

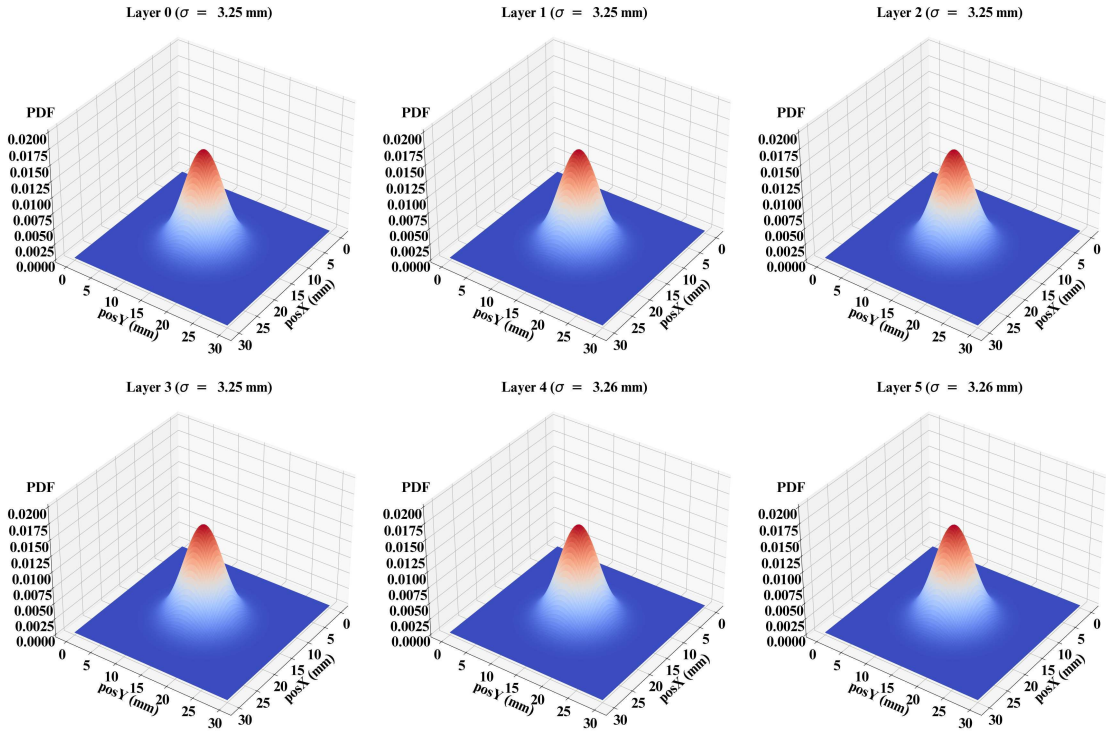

Figure 3.11 The 200 MeV pencil proton beam modeled by Gaussian distribution. The fitting parameters are calculated as shown in Table 3.3.

The deposited energy of protons in the epitaxial layer is determined in the same way as shown in Section 3.2.1. Ionisation of deposited energy produces electron-hole pairs in the epitaxial layer. Electrons move from the valence band to the conduction band, and holes move from the conduction band to the valence band. The phenomena is exploited to create an electrical signal. The number of electron-hole pairs is gathered as an active pixel signal in the ALPIDE sensor, and related to the energy deposition in the epitaxial layer.

In the simulations, pencil proton beams with energies of 70 and 200 MeV are defined as the simulation sources. The pencil proton beam passes through the ALPIDE sensor while transferring some energy to the material layers. Secondary particle creation can occur, and the material layers can receive some deposited energy from those secondary particles. As a result, only proton particle energy deposition is seen using filter Tree hit data with parentID 0 as indicated in Section 3.2.4.

The distribution of energy deposition in each detector plane is similar in both

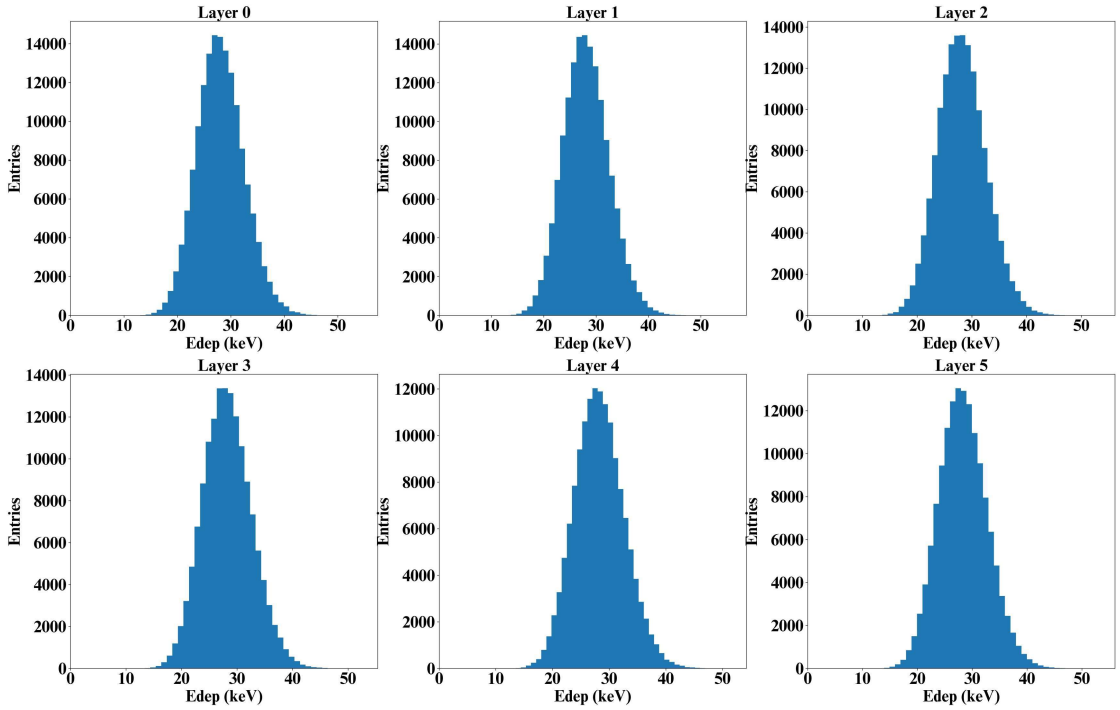

Figure 3.12 The distribution of proton energy deposition in epitaxial layer of ALPIDE sensor with 70 MeV pencil beam source

Table 3.4 The mean and standard deviation (sigma) of proton particles deposit energy in epitaxial layer of ALPIDE sensor.

Plane no.	70 MeV		200 MeV	
	Mean (KeV)	Sigma (keV)	Mean (keV)	Sigma (keV)
0	28.0	4.39	13.0	2.96
1	28.1	4.38	13.0	2.95
2	28.2	4.40	13.0	2.94
3	28.3	4.39	13.0	2.95
4	28.3	4.40	13.0	2.95
5	28.3	4.40	13.0	2.94

70 MeV and 200 MeV, according to Table 3.4. For six ALPIDEs, the average means of deposit energy in epitaxial layer for 70 MeV and 200 MeV proton beams are 28.2 keV and 13.0 keV, and their average sigmas are 4.39 keV and 2.95 keV, respectively. The results reveal that energy deposition is affected by the energy of the beam source.

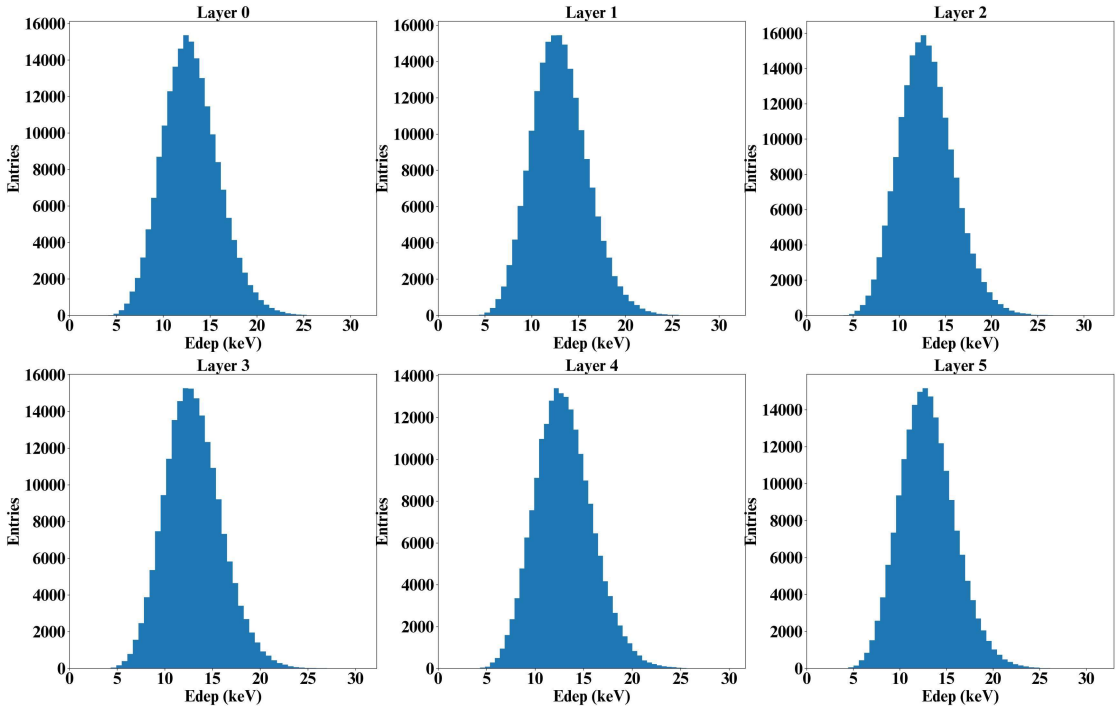

Figure 3.13 The distribution of proton energy deposition in epitaxial layer of ALPIDE sensor with 200 MeV pencil beam source

Lower energy has a higher likelihood of being absorbed by the sensor than high energy. Furthermore, the quantity of energy absorbed in the epitaxial layer reflects the size of the cluster, which is a group of activated pixel neighbors, as mentioned in section 5.4.2.

3.3.3 Proton track

When a charged particle passes through a detector, a trail of ionization or radiation is left behind, it can be picked up and recorded as a series of discrete points or hits. By combining these points or hits, one can determine its trajectory. In addition, a charged particle can also interact with the atomic nuclei or electrons inside the medium, causing its route to deviate from the incoming direction. The magnitude of the deviation is determined by charge and mass of the particle, as well as parameters of the material such as density and thickness.

The simulation data is converted into three-dimensional information for each sensor plane. To be identical with the experimental setup, the beam energies utilized in the simulation for reconstructing the track are 70 MeV and 200 MeV as described

in Section 3.2.2. The reconstruction algorithm will search for hits and connect them together to form the path. Because the exact track is collected along with the output data in MC simulation, the comparison between the MC track and reconstructed tracks implies the track reconstruction efficiency of this algorithm and can demonstrate the possibility of using this algorithm in the real experiment shown in chapter V. Three-dimensional hit data from simulations of 70 MeV and 200 MeV are given in Figure 3.14.

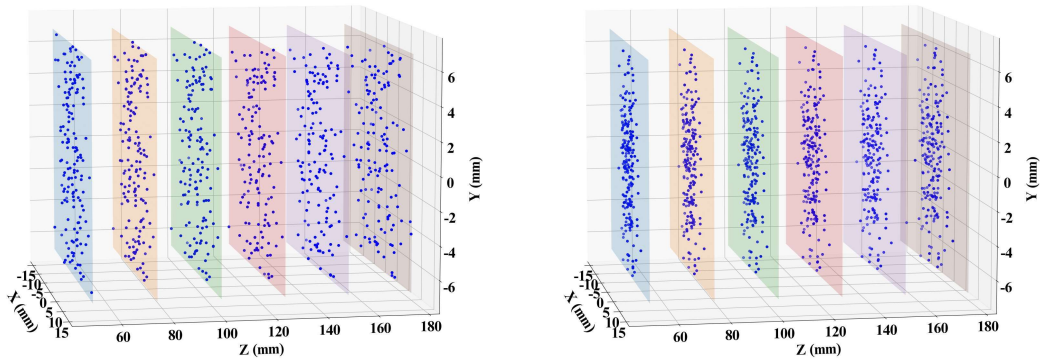

(a) 70 MeV. (b) 200 MeV.

Figure 3.14 3D hit data of simulations.

The track algorithm as described in Section 3.2.5 is applied to 3D hit data of both 70 MeV and 200 MeV. The S_{max} parameter is optimised by observing track efficiency on various primary events used in the simulation. The $\Delta\theta$ value, that is varied to determine the efficiency, is also compared to the σ_{θ_0} from Equation 3.4. According to the pCT prototype of the Loma Linda (Giacometti et al., 2017), the number of protons which are detected by detector per frame are required about 100 protons/frame in 1 cm^2 of sensor area. As reported by ALPIDE sensor area, the active space is 1.38 $\times$ 3.0 cm^2. So 400 primaries are evaluated in track reconstruction of the simulation part.

Figure 3.15 shows the track efficiency of 400 proton particles utilized in GATE/GEANT4 simulation using track efficiency equation 3.7, using 70 MeV and 200 MeV as energy sources. The S_{max} of 70 MeV and 200 MeV enable high efficiency of 80% and 100%, respectively, with a purity of 75%. In high efficiency zones, the cone angles for 70 MeV, and 200 MeV are 10 mrad and 1.5 mrad, respectively. The σ_{θ_0} is calculated

using Equation 3.4 and the radiation length values from Table 3.1 of Al + Si materials of single ALPIDE. The figure also demonstrates that at 70 MeV, about $5\sigma_{\theta_0}$ gives great track efficiency and $2\sigma_{\theta_0}$ at 200 MeV.

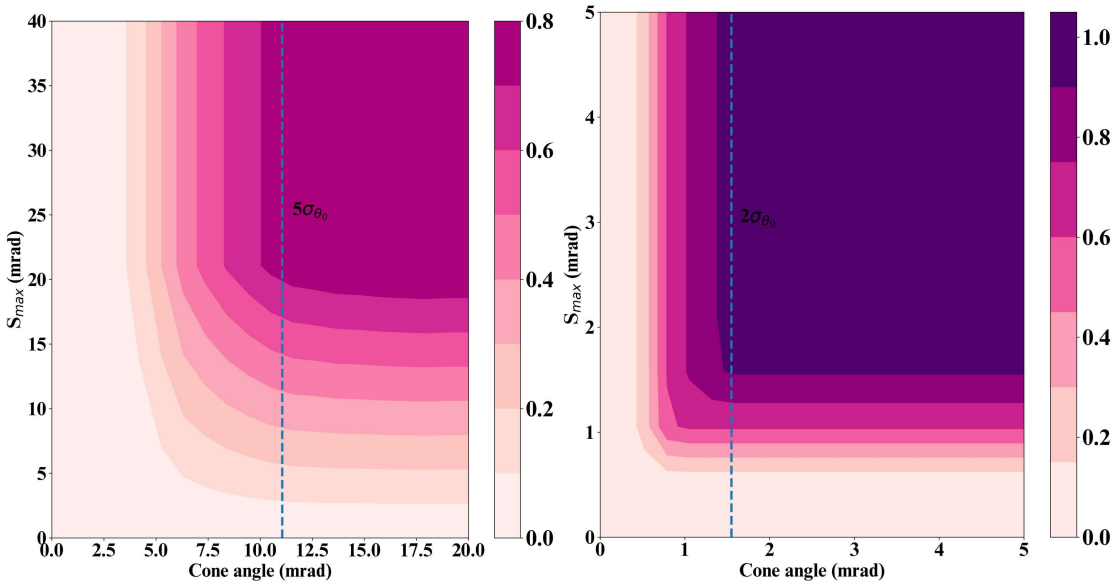

(a) 70 MeV. (b) 200 MeV.

Figure 3.15 The contour plot of track efficiency on various S_{max} and cone angle. The color bar of these plots show the reconstruction efficiency of tracking algorithm.

Figure 3.14 shows hit data visualization as 3D visualization. Figure 3.16 displays the track reconstruction result as a track path. The S_{max} and cone angle parameters utilized in the track reconstruction algorithm are taken from Figure 3.15 as 25 mrad of S_{max} and 11 mrad of cone angle for 70 MeV, and 2.0 mrad and 1.5 mrad, respectively, for 200 MeV. As a consequence, all proton tracks from the method applied to 400 simulated primaries are shown. Because the purity is set to 75%, some tracks do not connect candidates as six levels.

Instead of evaluating proton track efficiency based on the search cone angle and S_{max}, track efficiency can be thought of as the number of primary dependencies used in the simulation. The simulation in this section serves as a guideline for the experimental setup, and the simulation results can be used to uncover some requirements. Figure 3.17 depicts the track efficiency at 70 MeV and 200 MeV with different main numbers. When the primary is reduced to 70 MeV, the accuracy rapidly decreases. On the other hand, efficiency is declining slowly.

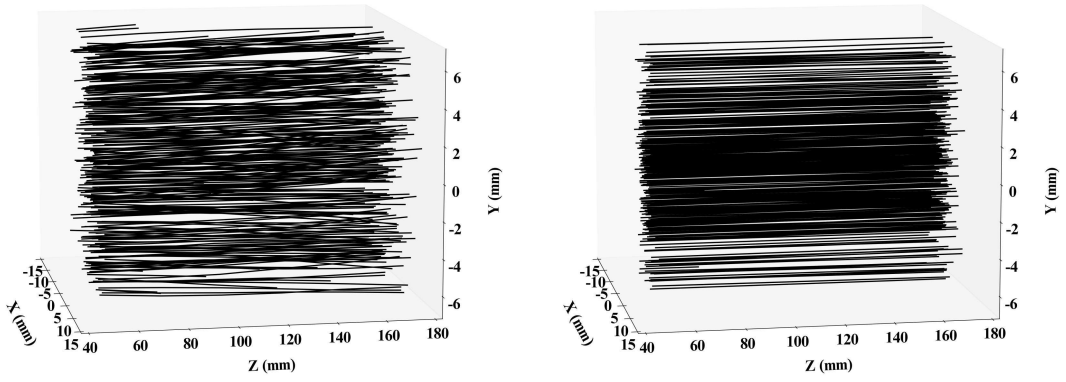

(a) 70 MeV. (b) 200 MeV.

Figure 3.16 GATE/GEANT4 simulation of 400 primary proton track routes. The tracks connect all candidates from layer 0 to the last layer, in which the last candidates of each track are discovered.

3.4 Summary

The simulation part evaluates the algorithm quality of the track reconstruction when applied to 3D hit data from Monte Carlo simulation. The geometry of the simulation model is based on an actual experiment conducted using an operating therapeutic proton beam at King Chulalongkorn Memorial Hospital (KCMH) in Thailand. Pencil Beam Scanning (PBS) is the beam, which can be represented by a two-dimensional Gaussian model. The simulation employs two beam energies. The lowest energy that can be irradiated from the KCMH cyclotron is 70 MeV, and the highest energy that can be evaluated by the transmission process is 200 MeV. For the test, 400 primaries are irradiated to the telescope. The epitaxial layer determines the deposited energy that causes the signal in a sensor. The electron-hole pairs are ionized by the absorbed energy in the material and produce the electrical signal. These signals can be represented as 3D hit data of particles striking a surface. Filtering only proton primary with parentID 0 from Tree hits in the root data file removes the secondary particles. The track efficiencies are estimated based on S_{max} and search cone angle of the reconstruction algorithm. Thus, the track following algorithm performs well in simulation at 20 mrad of S_{max} and

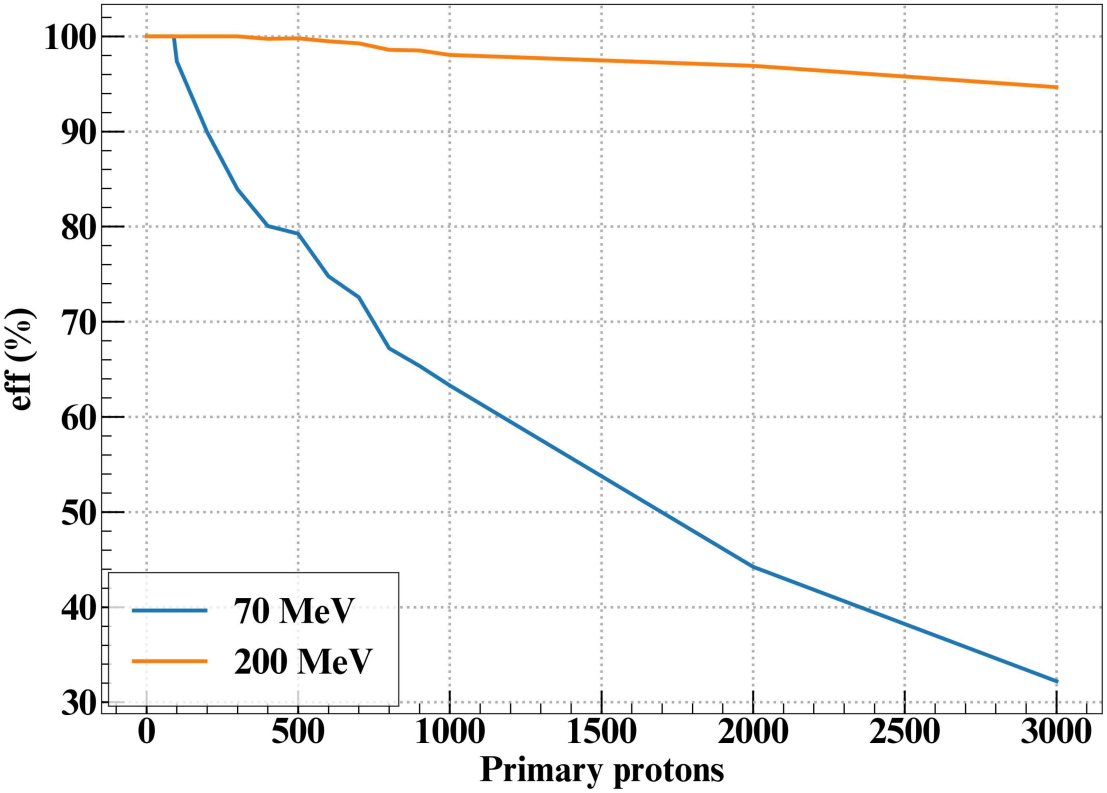

Figure 3.17 The track efficiency for proton sources at 70MeV and 200MeV depends on the number of primary protons employed in the GATE/GEANT4 simulation.

10 mrad of cone angle in 70 MeV and 1.5 mrad of S_{max} and 1.5 mrad of cone angle in 200 MeV. With the σ_{θ_0} calculation from Equation 3.4, the track efficiencies reveal that higher energy has more accurate track reconstruction than lower energy, and the S_{max} and cone angle values are narrower than 70 MeV when compared to σ_{θ_0} values of 200 MeV. Finally, when the number of primary factors affecting track efficiency is seen, a high intensity of the source implies a low efficiency.